Reconciling satellite-derived atmospheric properties with fine-resolution land imagery: Insights for atmospheric correction

Przemyslaw Zelazowski,[1] Andrew M. Sayer,[2,3,4] Gareth E. Thomas,[2] and Roy G. Grainger[2]

Received 10 December 2010; revised 28 June 2011; accepted 8 July 2011; published 30 September 2011.

[1] This paper investigates to what extent satellite measurements of atmospheric properties can be reconciled with fine-resolution land imagery, in order to improve the estimates of surface reflectance through physically based atmospheric correction. The analysis deals with mountainous area (Landsat scene of Peruvian Amazon/Andes, 72°E and 13°S), where the atmosphere is highly variable. Data from satellite sensors were used for characterization of the key atmospheric constituents: total water vapor (TWV), aerosol optical depth (AOD), and total ozone. Constituent time series revealed the season-dependent mean state of the atmosphere and its variability. Discrepancies between AOD from the Advanced Along-Track Scanning Radiometer (AATSR) and Moderate Resolution Imaging Spectroradiometer (MODIS) highlighted substantial uncertainty of atmospheric aerosol properties. The distribution of TWV and AOD over a Landsat scene was found to be exponentially related to ground elevation (mean R^2 of 0.82 and 0.29, respectively). In consequence, the atmosphere-induced and seasonally varying bias of the top-of-atmosphere signal was also elevation dependent (e.g., mean Normalized Difference Vegetation Index bias at 500 m was 0.06 and at 4000 m was 0.01). We demonstrate that satellite measurements of key atmospheric constituents can be downscaled and gap filled with the proposed "background + anomalies" approach, to allow for a better compatibility with fine-resolution land surface imagery. Older images (i.e., predating the MODIS/ATSR era), without coincident atmospheric data, can be corrected using climatologies derived from time series of satellite retrievals. Averaging such climatologies over space compromises the quality of correction result to a much greater degree than averaging them over time. We conclude that the quality of both recent and older fine-resolution land surface imagery can be improved with satellite-based atmospheric data acquired to date.

Citation: Zelazowski, P., A. M. Sayer, G. E. Thomas, and R. G. Grainger (2011), Reconciling satellite-derived atmospheric properties with fine-resolution land imagery: Insights for atmospheric correction, *J. Geophys. Res.*, *116*, D18308, doi:10.1029/2010JD015488.

1. Introduction

[2] The top-of-atmosphere (TOA) signal measured by a satellite imager includes contributions from both the surface and atmosphere. The difference between the TOA reflectance and the surface reflectance is termed atmospheric bias. The main causes of this bias are atmospheric scattering and absorption, which vary substantially with time, space, and wavelength. In the case of dark targets depicted in the visible part of the spectrum, the signal from the atmosphere may even exceed the signal from the surface. The majority of atmospheric constituents responsible for these effects are concentrated below approximately 3 km in altitude [*Vermote et al.*, 1997b]. Therefore, the resulting atmospheric bias of surface reflectance varies with ground elevation, an effect most evident in mountainous environments, which constitute about one quarter of global land surface [*Körner*, 2007]. Such bias can introduce error in discrete depictions of land surface, such as land cover classes [*Lu and Weng*, 2007], as well as in continuous ones, such as vegetation indices [*Myneni and Asrar*, 1994]. In the case of time series of measurements, the temporal variability of atmospheric properties can further deteriorate information about ground surface [*Coppin et al.*, 2004; *Kaufman*, 1985]. Atmospheric correction is, therefore, a key step in the preprocessing of optical satellite sensor

[1]Environmental Change Institute, School of Geography and the Environment, University of Oxford, Oxford, UK.
[2]Atmospheric, Oceanic, and Planetary Physics, Department of Physics, University of Oxford, Oxford, UK.
[3]Also at Remote Sensing Group, STFC Rutherford Appleton Laboratory, Chilton, UK.
[4]Now at Climate and Radiation Branch, Laboratory for Atmospheres, NASA Goddard Space Flight Center, Greenbelt, Maryland, USA.

0148-0227/11/2010JD015488

imagery, upon which depends the quality of image-derived products.

[3] Routinely performed atmospheric correction could increase the value of fine-resolution satellite data describing the Earth's surface, including the unequaled 30+ yearlong, freely available Landsat record [*Chander et al.*, 2009]. However, the correction burden has been largely placed on the user community, which has not always taken up the challenge. Potentially, the most accurate tools that have been applied in atmospheric correction are radiative transfer codes (RTCs) [*Kokhanovsky et al.*, 2010a; *Kotchenova et al.*, 2008], although they are generally designed to resolve a single case of land-atmosphere interaction, whereas in practice, a satellite scene includes many different cases. More importantly, in contrast to the precision of RTCs, the parameterization of the atmosphere over the fine-resolution satellite scene is usually much less accurate, which reflects both the quality and incompatibility issues in underlying atmospheric information.

[4] A number of techniques to estimate the amount of atmospheric bias from fine-resolution land surface images themselves have been developed to date. These methods usually address molecular and aerosol scattering [e.g., *Lyapustin et al.*, 2004; *Richter et al.*, 2006], whereas the estimation of atmospheric absorption, including its important component caused by water vapor, requires specific narrow spectral channels [*Gao and Kaufman*, 2003]. It can be concluded that the vast majority of fine spatial resolution sensors are not designed to simultaneously characterize land and atmosphere due to spectral characteristics of their bands, which is reflected by the lack of operational fine-resolution atmospheric data. On the other hand, there has been an increasing supply of lower-resolution satellite imagery more suitable for the retrieval of atmospheric properties, derived using sensors designed especially for this purpose. For example, the Moderate Resolution Imaging Spectroradiometer (MODIS) [*Levy et al.*, 2010], Medium Resolution Imagine Spectroradiometer [*von Hoyningen-Huene et al.*, 2003], and Ozone Monitoring Instrument (OMI) [*Levelt et al.*, 2006; *Schmid et al.*, 2009] have provided daily near-global coverage for approximately one decade (note that OMI-like ozone data have been acquired since the late 1970s). The Along-Track Scanning Radiometers (ATSRs) [*Llewellyn-Jones et al.*, 2001] and Multiangle Imaging Spectroradiometer [*Martonchik et al.*, 2002] have provided about weekly near-global coverage for over a decade. Therefore, for every place on the planet, there is an increasing potential not only to characterize the atmosphere at the time of acquisition, but also to describe its mean state and seasonality. In the context of atmospheric correction, this potential is especially important in the case of atmospheric aerosol, water vapor, and possibly also ozone, which are the most variable atmospheric constituents (other than clouds, the presence of which generally precludes measurement of surface properties all together).

[5] This paper considers to what extent satellite measurements of these key atmospheric properties can be reconciled with fine-resolution satellite imagery of land surface in order to improve estimates of surface reflectance through physically based atmospheric correction. By fine-resolution, we mean any imagery with spatial resolution higher than that of satellite-based products describing the atmosphere. The proposed "background + anomalies" approach is applied in interpolation and gap filling of such products, so that atmospheric data become more compatible with land surface imagery, which is demonstrated with Landsat data (spatial resolution, 30 m). We also investigate the link between the amount of atmospheric constituent and the ground elevation, which plays an important role in the proposed approach. We then evaluate various strategies of atmosphere parameterization, for the cases in which atmospheric data coinciding with a particular Landsat acquisition are available (recent acquisitions), or not (old acquisitions, predating the MODIS/ATSR era). In the latter case, time series of available data provide information on the season-dependent mean state of the atmosphere and the range of atmospheric variability.

2. Methods

2.1. Research Area, Data Sources, and Analysis

[6] This study focuses on the variability of atmosphere over a single, yet highly diverse, Landsat scene (path 4, row 69, centered at 72°E and 13°S), depicting the western fringe of the Amazon and the eastern Peruvian Andes. The scene's area (185 × 185 km) represents contrasting cases of interaction between light, atmosphere, and land, which result from a high range of ground elevations (270–6300 m above sea level), aerosol loadings, and land cover types.

[7] The key atmospheric constituents over this scene were characterized using satellite data from three sensors (Table 1): MODIS Terra-aerosol optical depth (AOD) and total water vapor (TWV), Advanced ATSR (AATSR)-AOD, and OMI-total ozone (TO). Spatial resolution of these estimates is, in all cases, much coarser that the 30 m resolution of Landsat ETM+ optical bands considered in this study. The reason for using aerosol data from more than one source was that its retrieval is the most challenging among the analyzed constituents; hence, the estimates can be expected to vary between sensors.

[8] The analysis of atmospheric contents focused on two contrasting elevation ranges, 250–750 m ("500 m") and 3750–4250 m ("4000 m"), as depicted in the Shuttle Radar Topography Mission data (SRTM version 4, accessed at http://srtm.csi.cgiar.org). These elevations correspond to Peruvian lowland Amazon forests and to *puna* grasslands just above the tree line, respectively. In the case of low-resolution TO data, such contrast of elevations could only be achieved with measurements taken to the east and west from the research area. The high range of available ground elevations allowed investigation of regional vertical profiles of the most variable constituents, AOD and TWV. To illustrate the predictive power of elevation for their amounts, a coefficient of determination (R^2) was calculated for each data granule.

[9] Time series and climatologies, based on the above described data, were applied in the analysis of atmospheric bias of the TOA signal, performed with the 6S RTC [*Kotchenova and Vermote*, 2007; E. Vermote et al., Second simulation of a satellite signal in the solar spectrum-vector (6SV), 6S user guide, version 3, http://6s.ltdri.org/6S_code2_thiner_stuff/6s_ltdri_org_manual.htm, 2006]. This part of the analysis enabled the assessment of variability of reflectance due to changing atmosphere and illumination only,

Table 1. Characteristics of Data Sources Used in Derivation of Time Series of Atmospheric Properties

Characteristics	Atmospheric Constituent			
	Aerosol Optical Depth		Total Water Vapor	Total Ozone
Sensor	AATSR	MODIS Terra	MODIS Terra	OMI
Years analyzed	2003–2008	2002–2008	2002–2008	2004–2009
Acquisition time	~10:30 UT (solar)	~10:00 UT (solar)	~10:00 UT (solar)	~14:00 UT (solar)
Frequency	Every 4 days	Daily	Daily	Daily
Spatial resolution	10 km	10 km	1 km	1 arc degree (~108 km)
Data set	ORAC [*Thomas et al.*, 2009]	MOD04_L2 Collection 5; Optical_Depth_Land_And_Ocean	MOD05_L2 Collection 5; Water_Vapor_Near_Infrared	OMTO3; (TOMS algorithm version 8.5)
Quality threshold	As by *Sayer et al.* [2011]	Quality assurance flag = 3	Quality assurance flag > 2	All data

since surface characteristics (vegetation described with spectral signature provided with 6S) were kept constant. Aerosol type was assumed to be "biomass burning," based on field observations [*Zelazowski*, 2011] and literature [e.g., *Bush et al.*, 2008]. The amounts of other atmospheric constituents were automatically estimated by 6S based on ground elevation. Atmospheric bias was estimated for Landsat ETM+ sensor bands 1–5 and 7. Normalized Difference Vegetation Index (NDVI), one of the most commonly used satellite-based characteristics of the land surface [*Pettorelli et al.*, 2005], was calculated based on bands 3 and 4. A supplementary factorial analysis, performed for the case of maximal 15 day mean amounts of atmospheric constituents and across the whole optical spectrum, allowed an illustrative breakdown of atmospheric bias into contributions from particular atmospheric effects: scattering and absorption by aerosol, absorption by water vapor, absorption by ozone, and other molecular absorption and scattering.

[10] The effects of surface Bidirectional Reflectance Distribution Function (BRDF) and varying Landsat scan angle were not incorporated in the above analysis. Instead, their impact was assessed in a separate set of simulations with BRDF data extracted from the MODIS MCD43B1 product (accessed at http://wist.echo.nasa.gov) for the forested parts of the research area.

[11] In addition to the above simulations, which focused on the variability of TOA signal attributable to the atmosphere, a series of 10 relatively cloud-free Landsat 7 images were analyzed before and after atmospheric correction. Cloudless pixels that were common to all images and fell within the two elevational bands of interest (21,974 and 543,788 pixels at elevations near 500 and 4000 m, respectively) were used in visualization of real cases of surface reflectance and its atmospheric bias, both changing in time. Atmospheric correction was performed with a set of Matlab routines (http://www.eci.ox.ac.uk/research/ecodynamics/landcor/) that allow application of 6S to each image pixel, taking account of local atmospheric conditions, which were approximated with atmospheric data downscaled and gap filled with the background + anomalies approach (see below).

2.2. The Assumed Model of Constituent's Spatial Distribution

[12] Among the three analyzed atmospheric constituents, TO was assumed not to vary with ground elevation across a Landsat scene, as its majority resides in the stratosphere [*Randel et al.*, 1999]. In contrast, TWV and AOD were assumed to depend on ground elevation, since the majority of these constituents are located in the lower troposphere [*Vermote et al.*, 1997a], and this dependence has been documented over the research area with a Sun photometer [*Zelazowski*, 2011] and in other regions with airborne lidars and spectrometers [e.g., *He et al.*, 2008; *Livingston et al.*, 2003; *Turner et al.*, 2001]. Therefore, an adequate representation of the TWV and AOD distribution across a Landsat scene can be expected to often require higher spatial resolution than available in satellite-derived products. This distribution was assumed to consist of two components. The first component is the background concentration, which reflects the portion of the constituent that is well diffused in the air, and has three properties: (1) it strongly depends on ground elevation, (2) it is date specific, and (3) it has an altitudinal limit (where concentrations are negligible). The second component represents anomalies, which can be linked to local sources of the constituent (e.g., fires in the case of atmospheric aerosol). This model of distribution will be referred to as background + anomalies approach (equation (1)):

$$C_{x,y,t} = B_t - L_t\left(E_{x,y}\right) + A_{x,y,t}, \tag{1}$$

where C is the total constituent amount in the downscaled fine-resolution coverage of either TWV or AOD, at spatial coordinates x, y, and time t; B is the constituent amount at the lowest considered elevation (the base amount); $L(E)$ is the elevation-dependent lapse in the total amount of constituent; and A is the local anomaly, defined as the difference between the predicted amount ("background") and the actual amount retrieved from the satellite sensor. Note that the lapse could be expressed as dependent on atmospheric pressure, instead of elevation. This model is employed in the downscaling and gap filling of atmospheric satellite data, which enables better compatibility with land surface images. Goals of this analysis include testing the validity of such an approach and finding an optimal way to parameterize it. It should be noted that this approach yields results very different to simple interpolation, which does not take advantage of the explanatory power of ground elevation. When anomalies (based on low-resolution data) are added to a fine-resolution background, the topography-linked detail is preserved. In this analysis, coverages of local anomalies were interpolated (bilinearly), and then smoothed, before combining with the background concentration, which is a simple remedy to unrealistically sharp transitions.

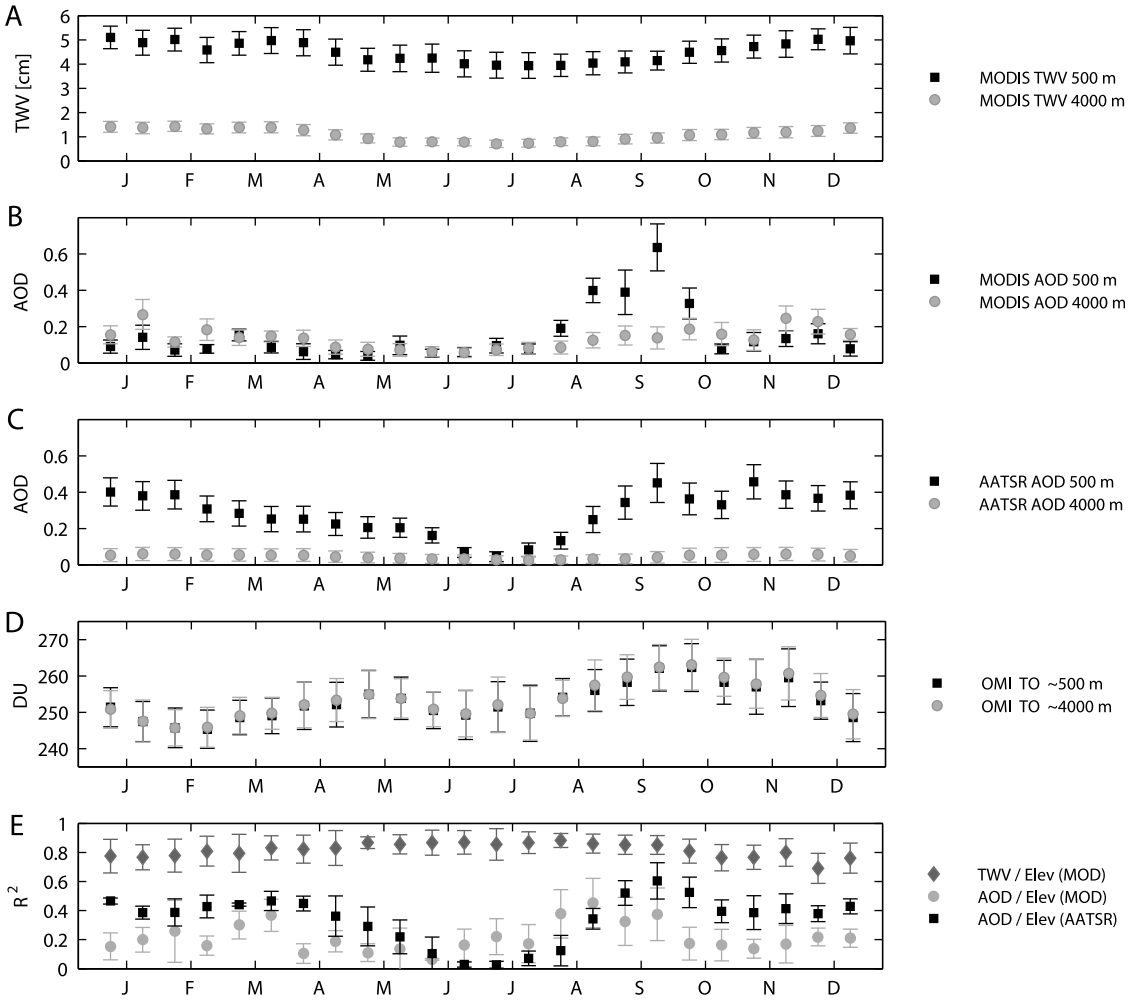

Figure 1. Climatology of atmospheric constituents (mean ± standard deviation) in the case of (a) AOD from MODIS, (b) AOD from AATSR, (c) TWV from MODIS, and (d) TO from OMI. Black squares and gray circles represent amounts at low (500 ± 250 m) and high (4000 ± 250 m) ground elevation, respectively. (e) The strength of ground elevation as a predictor of constituent amount (coefficient of determination; R^2).

[13] Amounts of other major atmospheric constituents (atmospheric gases) are also required for atmospheric correction, and they were assumed to be uniformly mixed in the atmosphere. Therefore, their concentration can also be described by the above model, but without the "anomalies" component.

2.3. Strategies to Parameterize the "Unknown" Atmosphere

[14] The following strategies to approximate atmospheric composition were considered for atmospheric correction of old satellite images (i.e., predating the MODIS/ATSR era) and large parts of newer images, for which coinciding satellite data on atmosphere are not available (small data gaps can be dealt with the background + anomalies approach):

[15] 1. "Pristine air" does not take into account the most date- and space-dependent atmospheric constituents: atmospheric aerosol and water vapor, but it resolves scattering and absorption attributable to the rest of the (molecular) atmosphere. TO was assumed to equal 0.25 cm. This strategy could be used when virtually no data on AOD and TWV are available; although a generally better strategy is to assume a nonzero content of these estimates. The main reason for using this approach was to estimate the contribution of AOD and TWV to atmospheric bias of reflectance.

[16] 2. "Full climatology" parameterizes the three considered atmospheric constituents based on their average annual cycles derived from satellite data and described in 15 day steps.

[17] 3. "Spatially averaged climatology" takes account of the season-dependent variability in atmospheric constituents, as in the Full climatology approach. However, the amounts of all constituents have been averaged spatially over the entire Landsat scene, which, in this case, led to parameterization typical for the atmosphere at a ground elevation of 2050 m. This strategy exemplifies a situation where the entire satellite scene is atmospherically corrected with a single run of the radiative transfer code.

[18] 4. "Temporally averaged climatology" takes account of the spatial variability of the atmosphere, but the amounts

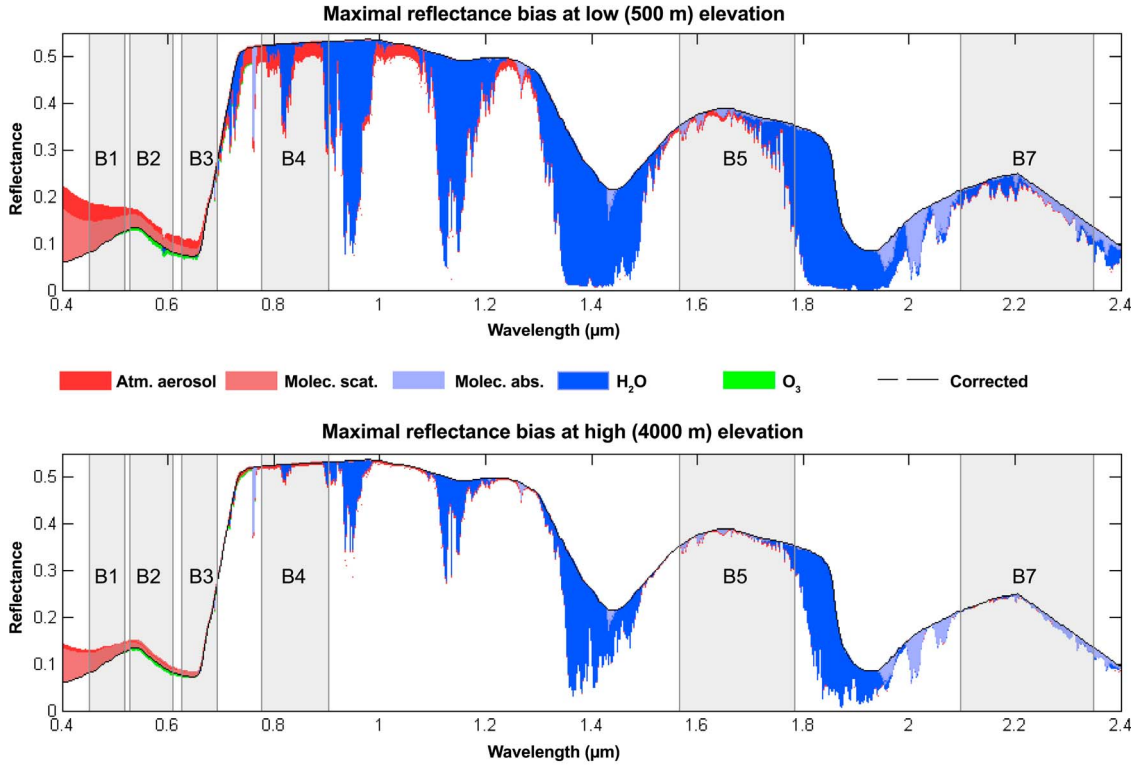

Figure 2. A breakdown of atmospheric bias across spectral signature of vegetation (black line) at low (500 m) and high (4000 m) ground elevation, simulated for the period with the highest mean amounts of atmospheric constituents (as depicted in Figure 1). Shaded areas mark spectral extent of the Landsat 7 sensor bands.

of considered constituents are equal to their long-term means. This strategy can be seen as an easily achievable improvement over the Pristine air strategy.

[19] These approaches were subsequently evaluated in terms of their effectiveness in removing atmospheric bias from reflectance estimates. All of them can be used in combination with the background + anomalies approach; however, note that anomalies can only be mapped based on atmospheric data acquired at the same time as the image to be corrected (or based on the image itself).

3. Results

3.1. Temporal and Spatial Distribution of Key Atmospheric Constituents

[20] Climatologies of atmospheric constituents (season-dependent mean states and variability), derived from time series of satellite data, appear as robust and distinct (Figures 1a–1d). TWV exhibits clear seasonality, with the lowest values falling in the dry season (June–August). The mean amounts change by ~20% at low elevations (from 5 to 4 cm), and by ~50% at high elevations (from 1 to 0.5 cm) in a yearly cycle. In contrast (also to AOD), TO fluctuates by only about 10% and is practically the same at high and low elevations. Despite this low variability, the seasonality of ozone is also well pronounced (i.e., the 15 day means have small standard deviations). The climatologies of AOD, depicted by MODIS and AATSR data, are quite different (Figures 1b and 1c). Both sensors show a peak in AOD (up to ~0.6) at low elevations, starting in the middle of the dry season, when the TWV is at its yearly low. However, in MODIS data, the peak is more pronounced and lasts for just above 2 months, whereas in AATSR data, the elevated AOD persists until February and subsequently falls steadily until July. In the case of high elevations, AATSR AOD is consistently low, but the MODIS AOD mean values are substantially higher, reaching up to ~0.25, and often exceed the means from low elevations. Based on fire risk data (no risk from November [*Bush et al.*, 2008]), the inspection of a series of Landsat images, and AOD product literature and documentation [*Levy et al.*, 2010; *Thomas et al.*, 2009], it was concluded that both sensors respond to elevated smoke levels due to fires, but the AATSR retrievals are probably more sensitive to contamination by small clouds (due to the instrument's coarser native spatial resolution), whereas MODIS retrievals have a positive bias at high elevations, as reported for other mountainous areas. This led to the decision that the further analysis of atmospheric bias will focus on simulations performed for low elevation with data from MODIS and for high elevation with data from AATSR.

[21] Time series of coefficient of determination (R^2; Figure 1e) show that the amount of variance that can be explained by ground elevation is consistently high in the case of TWV (0.7–0.9) and the dry season values are the highest. In the case of AOD, R^2 is generally lower, but also more seasonal, with a clear drop of R^2 in the AATSR data, a trend opposite to that of TWV data. Comparison between these results and the mean AOD (Figures 1b and 1c)

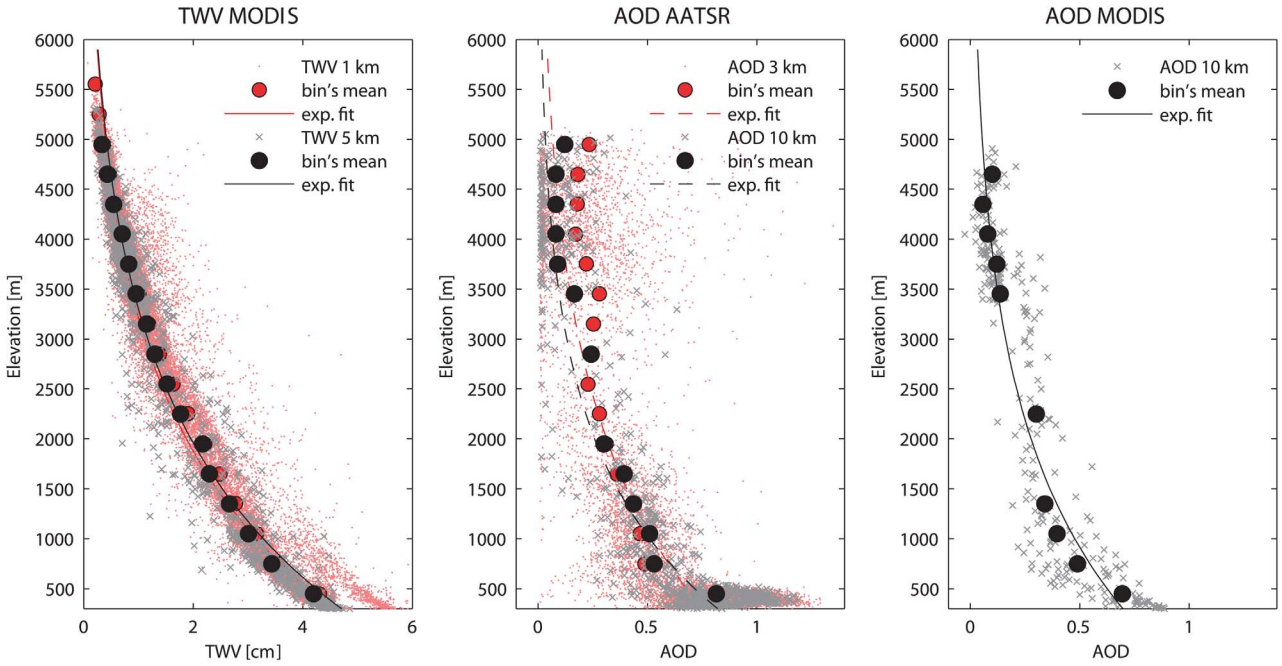

Figure 3. An example of strong dependence of TWV and AOD on ground elevation on a clear day with relatively high AOD (14 September 2007). Black and red circles mark averages from 300-m-wide ranges in elevation (bins), calculated only when >10 measurements were available.

revealed that the coefficient of determination largely reflects the degree of contrast between low and high elevations, which is always high only in the case of TWV. This suggests that low R^2 does not necessarily signify a weak elevation dependence of the background concentration, but rather that this background is consistently low across the whole elevation gradient. Moreover, in the case of MODIS AOD, the elevated retrievals at high elevations can partly explain the relatively lower R^2 in the dry season but also its elevated values during the rest of the year, when an apparent inverse relationship with elevation may occur.

[22] The above mentioned temporarily variable atmospheric constituents, along with the other gaseous components of the atmosphere, distort the signal from land surface. The effect of these components, at 0.5 and 4 km ground elevation, has been visualized in Figure 2, for the case of the maximum 15 day mean amounts of constituents found over the research area and the standard spectral signature of green vegetation. TO overall has only a minor, diminishing effect on the spectral signature, mainly in the range of Landsat's band 2, but also the adjacent bands. This, and the fact that TO exhibits a relatively small date-dependent variability (Figure 1), suggests that over the investigated region its long-term mean is a sufficient parameter for atmospheric correction. In contrast, atmospheric aerosol and water vapor can have a major influence on the signal registered by all Landsat bands. Aerosol increases the apparent signal of vegetation in the visible spectrum and decreases it in the infrared, whereas water vapor only decreases the apparent signal in the infrared. Because vegetation reflectance tends to be relatively small in the visible, the role of atmospheric scattering (atmospheric aerosol included) in biasing the signal is relatively large.

[23] The presented evidence underlines the importance of TWV and AOD, their variability across time (Figure 1), and the impact on surface reflectance retrievals across the light spectrum (Figure 2). Further analysis focused on the spatial variability and the relationship between these constituents and ground elevation, a key element of the background + anomalies approach, using data granules acquired during clear days, with ≥50% of the research area covered by retrievals (TWV, 7% of days; AOD AATSR, 2% of days; AOD MODIS, 3% of days). Figure 3 presents an example based on data granules from 14 September 2007. The exponential model fitted to the data performs better than a linear one (here R^2 is 0.95 versus 0.92 in TWV 1 km, 0.96 versus 0.92 in TWV 5 km, 0.573 versus 0.572 in AOD AATSR 3 km, 0.75 versus 0.74 in AOD AATSR 10 km, 0.78 versus 0.77 in AOD MODIS), whereas on dates with fewer available retrievals, the exponential fit is likely to not appear as better than the simple linear one. The exponential decay of constituent amount in a well-mixed atmosphere can be linked to the exponential decrease in atmospheric pressure. The exponential curve underestimates the amount of constituent at the lowest elevations (Figure 3, middle and right), but to a degree markedly smaller than it would be in the case of a linear fit. In the presented case, as well as in the entire data set, the near-zero concentration of TWV occurs from ~6 km (average value of 0.007 cm), and it is systematically higher than in the case of AOD, for which there were virtually no positive retrievals above the elevation of 5 km.

[24] The retrieved constituent-elevation relationship was found to be affected by the data set's spatial resolution. The TWV mean values, across the elevation gradient, differ only slightly with resolution (Figure 3, left). In fact, data aggregation improved quality, as a population of anomalously

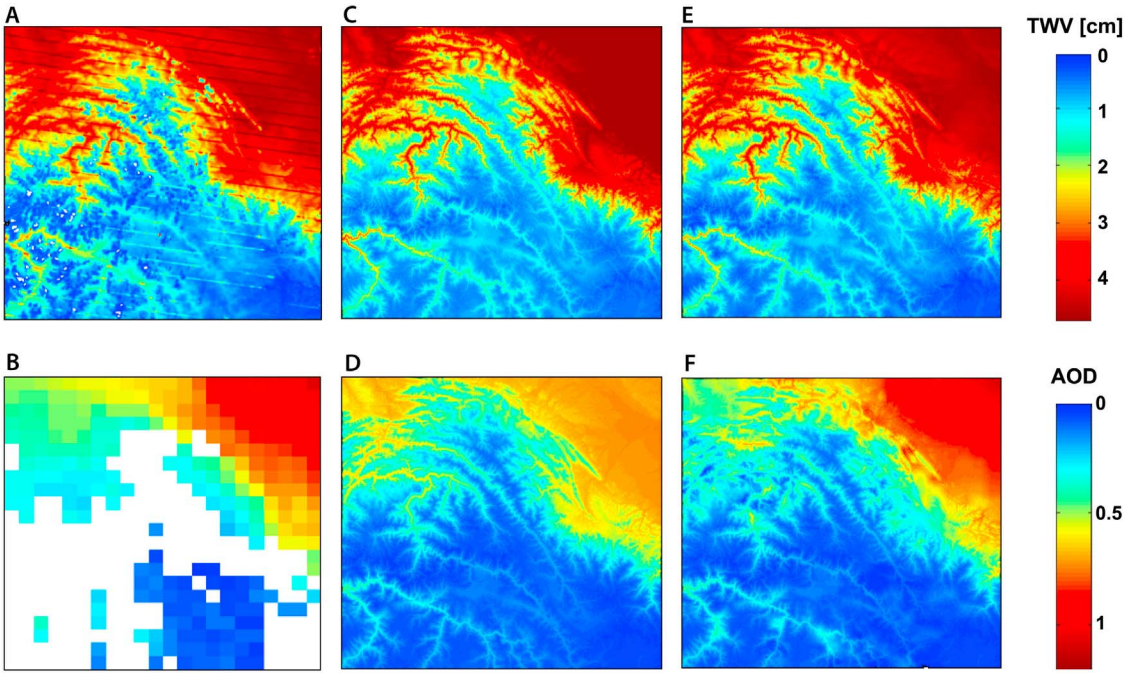

Figure 4. Satellite data from MODIS and fine-resolution coverages derived with the background + anomalies approach. (a and b) Unprocessed TWV and AOD data, respectively (also plotted in Figure 3). (c and d) Fine-resolution concentrations calculated using the constituent-elevation relationship based on all data points (background). (e and f) Coverages with the known departures from the background (anomalies) locally calibrated based on available satellite retrievals. More examples of such coverages, employed in atmospheric correction of Landsat imagery, are provided in the auxiliary material.[1]

high values was discarded. However, in the case of AOD (Figure 3, middle, AATSR data), especially at high elevation, the mean is markedly lower when depicted in coarser resolution. This difference could be a consequence of the varying representativeness of the data set (linked to the number of available retrievals), as well as the procedure of data aggregation. The role of these effects can be expected to be generally greater in data sets with lower spatial resolution.

3.2. Downscaling of Atmospheric Constituent Data

[25] The steepest elevational gradients observed in the data set were ~0.1 and ~1.1 cm/km for AOD and TWV, respectively. Depicting such gradients over the Landsat scene of rugged terrain with the same accuracy as in the atmospheric product requires high spatial resolution. This section demonstrates the application of the background + anomalies approach in downscaling and gap filling of the atmospheric data.

[26] Figure 4 shows gridded CWD and AOD data (the same as shown in Figure 3) in their original form (Figures 4a and 4b), as well as processed data using the proposed approach (Figures 4c–4f). The so-far presented TWV data suggest that even the basic distribution model, consisting of only the background component, can be sufficient to capture the date-dependent spatial variability. Such an approach (Figure 4c) allowed not only for higher-resolution coverage but also for the removal of stripes with erroneous data (also visible in Figure 3). However, the full background + anomalies approach (Figure 4e) allowed for further benefit of mapping the regions that does not conform to the background formulas, through local calibration of the downscaled data using available satellite retrievals. This mitigated the overprediction of TWV at the lowest elevations. It should be noted that the accuracy of such adjustment requires good spatial colocation between the elevation data and atmospheric constituent data.

[27] Application of the background + anomalies model to AOD data visualizes another important advantage of using this downscaling approach, which is the replacement of large data gaps with a probable background concentration of the constituent (Figures 4d and 4f). The need for gap filling is generally high in the case of all analyzed data sets; however, there are large differences in this regard. For example, in the daily MODIS-based retrievals, TWV was available for more than 10% of the research area on 56% of days, whereas AOD was available on 35% of days. The AATSR data were acquired over the research area on only 531 of 2196 considered dates (24%).

[28] The continuous fine-resolution coverages of atmospheric constituents can be applied in the atmospheric correction procedure, which takes account of their spatial variability. Figure 5 (left) shows TOA reflectances in a Landsat scene with conspicuous atmospheric bias that depends on elevation, whereas Figure 5 (right) depicts the same image corrected using multiple runs of 6S RTC that adequately addressed variability of land-atmosphere interactions.

[1] Auxiliary materials are available in the HTML. doi:10.1029/2010JD015488.

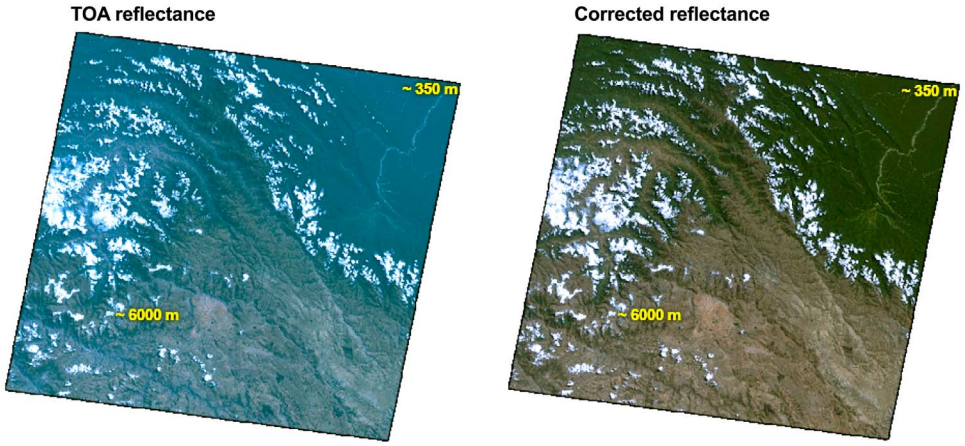

Figure 5. Landsat scene (centered at 72°E and 13°S), which defines the spatial boundaries of the study. (left) True color composite of TOA reflectances acquired by Landsat TM sensor on 1 September 2008. (right) The same image after atmospheric correction in a procedure that considered the variability of atmospheric conditions. Regions of the lowest and highest ground elevation are marked in yellow.

3.3. Correction Strategies and Their Effectiveness

[29] This section reviews the potential effectiveness of atmospheric correction with four strategies to parameterize the atmosphere over old imagery of land surface (i.e., predating the MODIS/ATSR era), or parts of newer images, with no corresponding atmospheric data (small gaps can be dealt with the background + anomalies approach). Atmospheric bias of reflectance and NDVI that remains after atmospheric correction is presented in Figure 6 (visible spectrum bands), Figure 7 (infrared spectrum bands), and Figure 8 (NDVI) and is summarized in Table 2. In the simulations underlying these results, all variation in the TOA signal is due to changes in the atmospheric composition (and, to a small degree, varying illumination) because spectral signature of the considered vegetation target was kept constant. In the real-case scenario, the atmosphere-driven and elevation-dependent oscillation of TOA reflectance could be confused with changes arising from vegetation phenology. Moreover, the same land cover type may exhibit different apparent spectral characteristics if it occurs at contrasting elevations. The atmosphere tends to elevate the signal in visible bands (Figure 6), which contrasts with the decrease in the infrared spectrum (Figure 7). Therefore, the NDVI is especially prone to be biased, as it combines those two opposite tendencies (Figure 8).

[30] Results from the Pristine air correction (i.e., the difference between simulated signal at TOA and after the Pristine air correction), which assume no AOD or TWV in the air, show that the amount of atmospheric bias linked to these two constituents decreases with elevation. At 0.5 km, these two constituents are responsible for 53% of atmospheric bias, but at the elevation of 4 km, their impact is relatively small (22%), except for the case of band 4 (86%) and in consequence also the NDVI (45%).

[31] The three other correction strategies parameterized the atmosphere using constituent climatologies derived from 6 to 7 year-long time series. In the case of old imagery, with no coinciding atmospheric data, the anomalies cannot be mapped.

[32] The Full climatology approach delivered the best results (an average reduction of reflectance bias by 83% and 98% at low and high elevation, respectively) as it takes into account both the spatial and temporal variability of atmospheric constituents. When the atmosphere needs to be parameterized across the whole elevation gradient present in the scene, the constituent distribution model proposed earlier (equation (1)) can be transformed to require only one parameter:

$$Ctwv_{x,y,t} = Btwv_t e^{-E_{x,y}(\log(Btwv_t)0.00017+0.00033)} \quad (2)$$

$$Caod_{x,y,t} = Baod_t e^{-E_{x,y}(\log(Baod_t)0.00026+0.00083)} \quad (3)$$

where *Btwv* (or *Baod*) is the projected base concentration at sea level, which varies with season. In this model, the lapse rate depends on that base concentration in a way that negligible concentration is always reached at the same elevation. If such model is based on relative elevation measured from the lowest land within the scene (i.e., not sea level), then the base concentration becomes concentration at that local minimum.

[33] The "Temporarily averaged climatology" approach leads to results that are almost as good as the Full climatology approach (an average bias reduction of 78% and 98% at low and high elevation, respectively). However, it should be noted that the difference between the two strategies depends on how well the constituents' climatologies can be described. In the presented case, the average concentrations across the elevational gradient were approximated as follows:

$$Ctwv_{x,y} = 6e^{-0.00066E_{x,y}} \quad (4)$$

$$Caod_{x,y} = 0.27e^{-0.0005E_{x,y}}. \quad (5)$$

Last, when the atmosphere over a satellite scene is parameterized based on its average elevation (equivalent to the state of atmosphere at the elevation of ~2050 m), the relatively poor result at low elevation (58% bias reduction) and extremely poor result at high elevation (an increase in atmospheric bias of band 4 and NDVI) can be interpreted as a

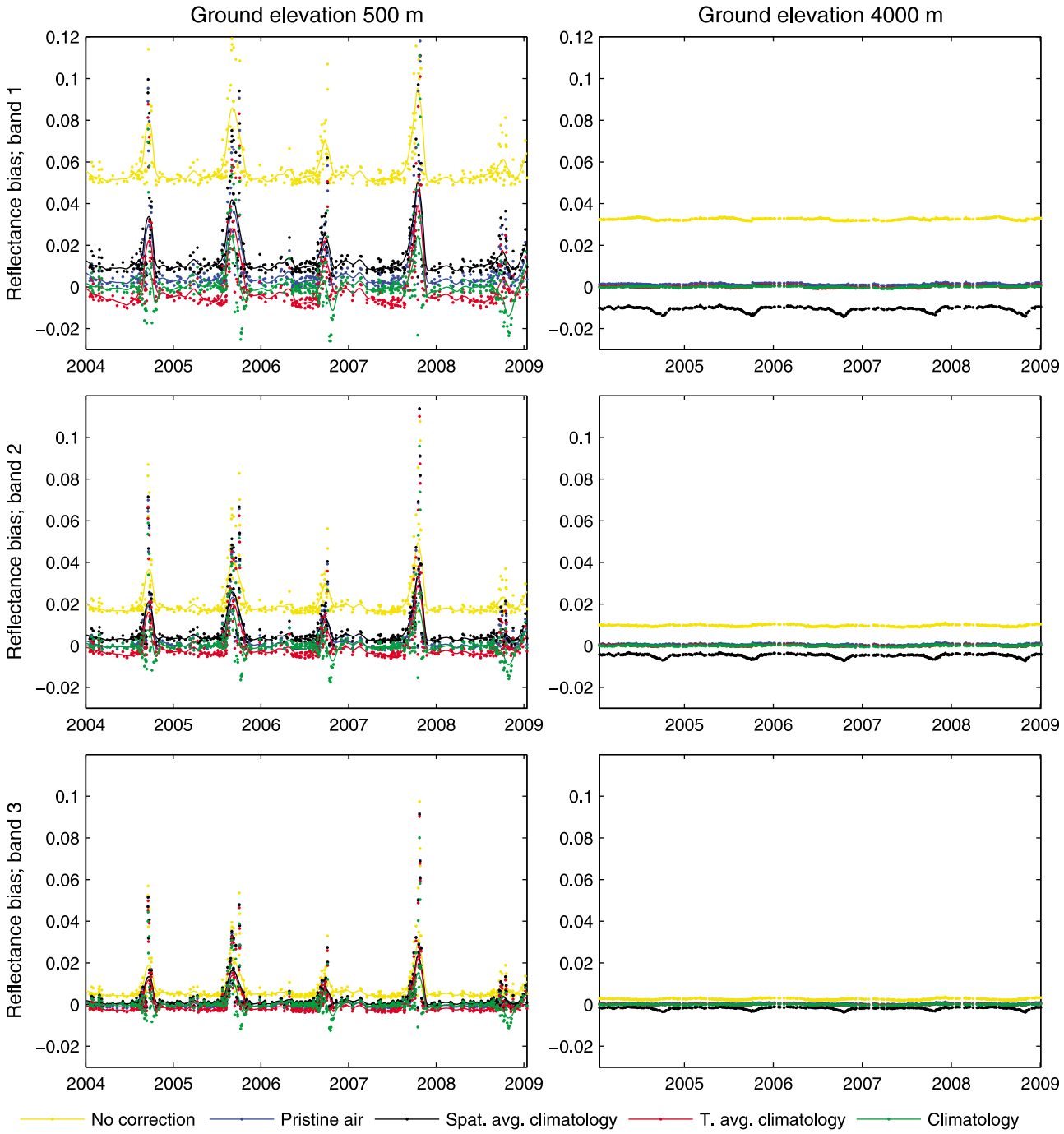

Figure 6. Atmospheric bias of green vegetation reflectance depicted by Landsat 7 bands within the visible spectrum (1, 2, 3) at low (500 ± 250 m) and high (4000 ± 250 m) ground elevation, as simulated with time series of data describing atmosphere and illumination conditions. Cases represent uncorrected reflectance (yellow) and reflectance corrected with four strategies using climatologies of atmospheric constituents presented in Figure 1. The strategies are applicable to imagery where the atmosphere at the time of acquisition is not known. (left) Individual simulations, as well as their 2 month moving average.

warning against atmospheric correction with only a single run of radiative transfer code, especially over highly rugged terrain.

[34] Additional simulations of atmospheric bias, which took into account surface BRDF and varying scan angle (15° field of view), enabled consideration of the "worst-case" scenario, which occurs over the image's eastern edge, where the sensor looks at forested land against the Sun and through a moist, aerosol-laden atmosphere (AOD = 1, TWV = 5 cm). In such a case, the assuming of nadir view at Lambertian surface across the whole scene led to underestimation of the atmospheric bias across the visible spectrum, maximally in band 1 (by 0.04, or 31%). In contrast, the bias in infrared spectrum was overestimated, but by a smaller degree, with a

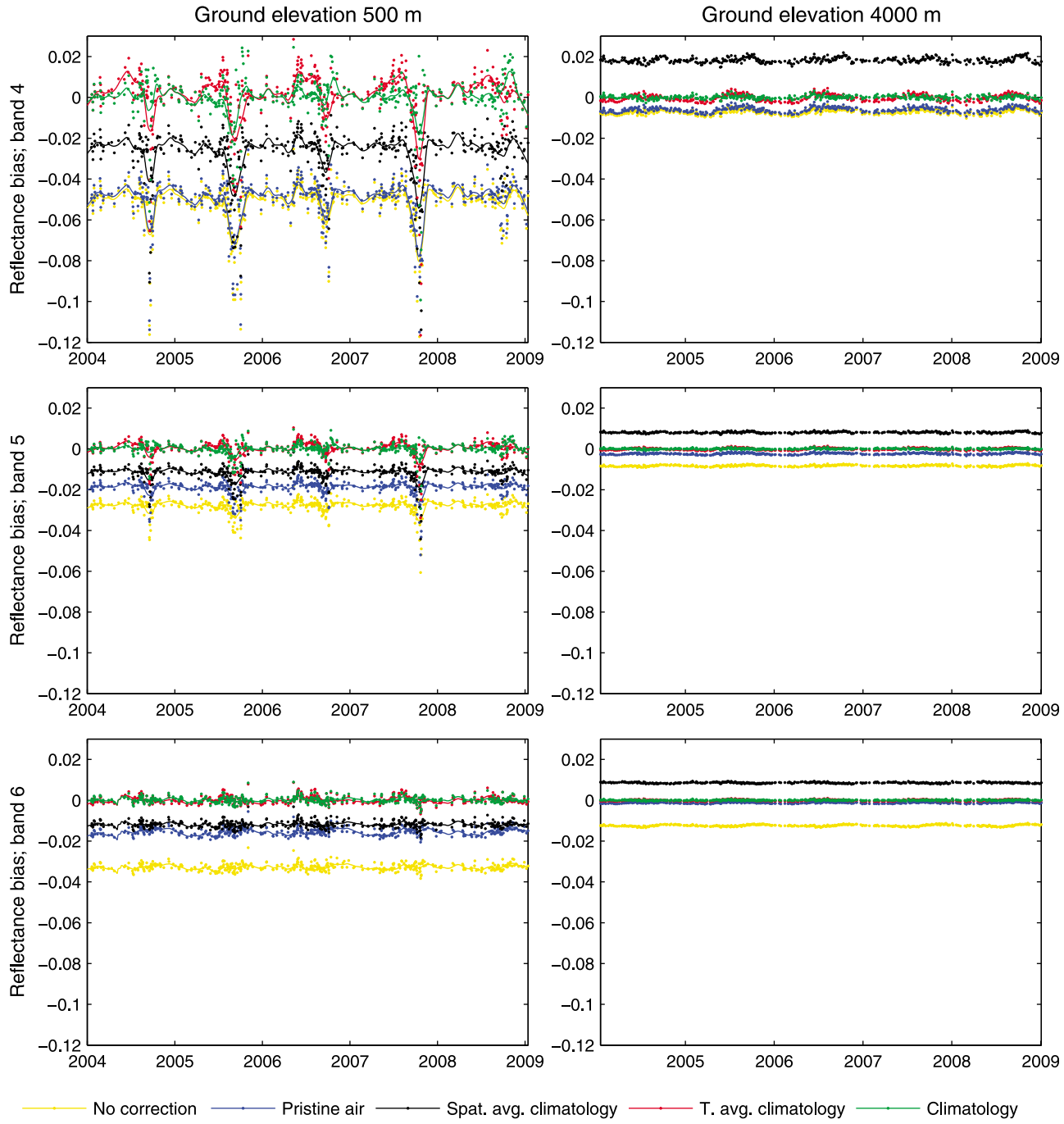

Figure 7. Atmospheric bias of green vegetation reflectance depicted by Landsat 7 bands within the infrared spectrum (4, 5, 7) at low (500 ± 250 m) and high (4000 ± 250 m) ground elevation. See the caption of Figure 6 for further information.

minimum in band 7 (0.002 or 5%). It was decided that these errors may be worth considering in the correction method, but they do not affect of the main conclusions of the study, especially since the reported values correspond to an extreme scenario.

[35] The last stage of this study focused on time series of Landsat 7 scenes acquired in years 2004–2008 (two scenes per year) and the visualization of real cases of surface reflectance and its atmospheric bias, both changing in time. All scenes come from the relatively cloud-free time-window between May and November, and each was corrected using available satellite data describing the atmosphere, after application of the background + anomalies approach. The most striking benefits of atmospheric correction are the restoration and temporal homogenization of information (Table 3 and Figure 9). The first aspect is illustrated by the shift in visible and infrared spectrum reflectance and in NDVI, which, to summarize data from Table 3, was much stronger at lower elevations (−62%, +10%, and +23%, respectively) than at higher ones (−29%, +2%, and +11%).

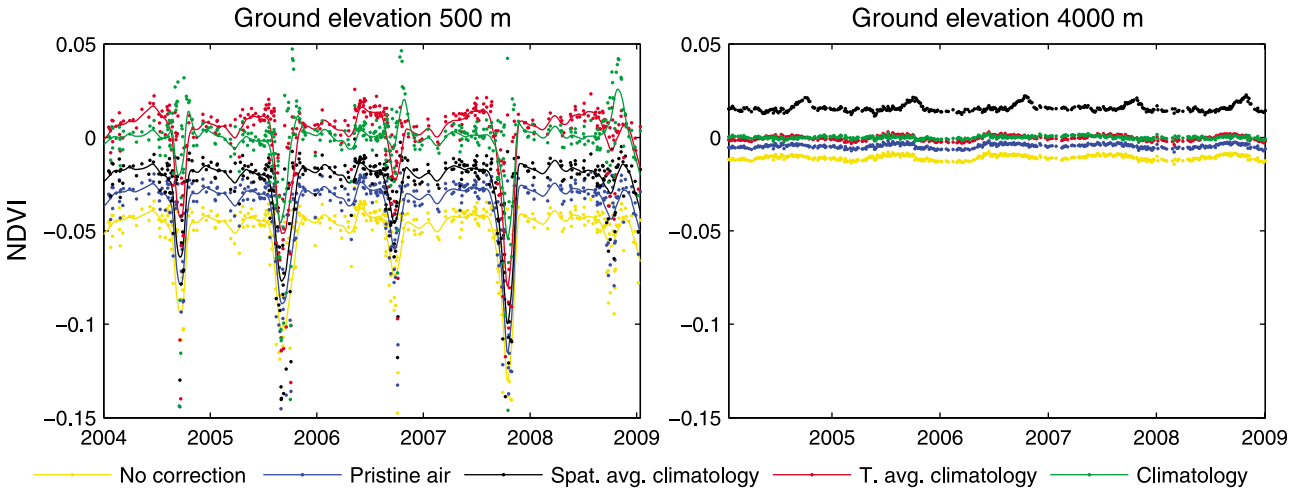

Figure 8. Atmospheric bias of green vegetation NDVI (0.63) at low (500 ± 250 m) and high (4000 ± 250 m) ground elevation. (left) The vertical axis was cropped for better data visualization (NDVI bias range, −0.15 to −0.4; 21 points omitted). See the caption of Figure 6 for further information.

Signal homogenization is documented by the strong decrease in standard deviation at low elevations (−81%, −5%, and −79%), accompanied by its small increase at high elevations (0%, +2%, and +8%). Another aspect of improved information after correction is the ratios between particular bands. For example, before atmospheric correction, bands 1 and 2 had values temporarily higher than band 5, which could substantially affect the results of land cover classification.

[36] By coincidence, signal from low and high elevations varied, to a similar degree, between dates. Atmospheric correction facilitated the finding that at low elevations, this variability largely reflected changes in atmospheric properties, especially AOD (Figure 9), whereas at the mountain tops, the change was largely driven by vegetation phenology (captured with NDVI) and possibly also seasonality of soil moisture, as suggested by the regular changes in bands 5 and 7.

4. Discussion and Conclusions

[37] This study shows that the majority of atmospheric bias in fine-resolution imagery of land surface can be corrected, even in the case of highly rugged terrain and unknown atmospheric properties at the time of scene acquisition. A prerequisite for correction is the generation of date- and region-dependent coverages of the most variable atmospheric constituents: AOD and TWV. Over a rugged terrain, these coverages can be downscaled with the proposed background + anomalies approach, which was shown to perform very well in the case of TWV and relatively well for AOD (see below). The spatiotemporal variability of TO over the research area was of negligible consequence for atmospheric correction quality, although it should be noted that at higher latitudes, the total amount and variability of ozone could be substantially greater [*Bowman and Krueger*, 1985].

[38] The study compared the effectiveness of different strategies to parameterize atmosphere for correction of reflectance. The assessment of correction accuracy needs to take into account the context of all errors characteristic to surface reflectance retrievals. These can be linked to (1) satellite sensor, (2) atmospheric data sets, and (3) the procedure to assess/remove atmospheric bias. The expected uncertainty of Landsat 7 TOA radiances is of 5% [*Chander et al.*, 2009], which could potentially make it the most important source of uncertainty, if most of the atmospheric bias is successfully corrected. The uncertainty of TO estimates (1%–2%; http://disc.sci.gsfc.nasa.gov/Aura/data-holdings/OMI/omto3_v003.shtml) is negligible because of the relatively low impact of this constituent on visible radiation. Error in TWV estimates (5%–10% [*Kaufman and Gao*, 1992; *Gao and Kaufman*, 2003]) is on the borderline of significance, given that TWV substantially impacts the absorption of infrared radiation. In the case of AOD, the reported uncertainty is substantial, both in the case of MODIS (±0.05 + 0.15 × AOD) [*Levy et al.*, 2010] and AATSR (estimated for each individual retrieval, but generally of a similar order of magnitude). Importantly, in some regions and seasons, the true error of AOD may exceed the expected error [*Levy et al.*, 2010]. Moreover, the relatively high spatial variability of AOD, coupled with frequent gaps in retrievals, affect the quality of downscaled and gap-filled data of the type presented in this study. In addition to this data set's uncertainty, the assumption of a particular aerosol type (its microphysical model) in a correction procedure can yield additional error because the estimate of AOD at wavelengths other than 550 nm depends on that assumption. Therefore, atmospheric aerosol, which is one of the most uncertain elements of the Earth's energy budget [*Forster et al.*, 2007], also appears to be the most important among the considered sources of error in the land surface retrieval. This uncertainty can exceed the error of surface reflectance retrieval that arises from neglecting surface BRDF (i.e., assuming Lambertian surface) and variability in scan angle, which can be largely resolved with realistic assumptions in the correction procedure. Nevertheless, the uncertainty of aerosol retrieval does not negate the benefits of the proposed atmospheric correction, because available AOD estimates, based on the best available knowledge, are almost certain to yield improvements in surface reflectance estimates. Moreover, other components of the atmosphere, which together are also a source of substantial atmospheric bias, can be characterized relatively well.

Table 2. Mean, Minimum, and Maximum Error of Vegetated Surface Reflectance and NDVI Due to Atmospheric Effects, Before and After Atmospheric Correction[a]

		Simulated Atmospheric Bias Time Series			
		Elevation 500 m		Elevation 4000 m	
Bands	Correction Strategy	Mean	(Min–Max)	Mean	(Min–Max)
Band 1 (0.099)	No correction	0.061	(0.049–0.188)	0.033	(0.032–0.034)
	Pristine air	0.011	(0.000–0.140)	0.001	(0.001–0.002)
	Spatially averaged climatology	0.017	(0.004–0.142)	0.011	(0.009–0.014)
	Temporally averaged climatology	0.010	(0.000–0.132)	0.000	(0.000–0.001)
	Full climatology	0.008	(0.000–0.111)	0.000	(0.000–0.001)
Band 2 (0.116)	No correction	0.023	(0.015–0.130)	0.010	(0.009–0.011)
	Pristine air	0.007	(0.000–0.114)	0.001	(0.000–0.002)
	Spatially averaged climatology	0.009	(0.000–0.114)	0.005	(0.003–0.007)
	Temporally averaged climatology	0.007	(0.000–0.110)	0.000	(0.000–0.001)
	Full climatology	0.005	(0.000–0.096)	0.000	(0.000–0.001)
Band 3 (0.125)	No correction	0.009	(0.003–0.097)	0.003	(0.002–0.004)
	Pristine air	0.005	(0.000–0.092)	0.000	(0.000–0.001)
	Spatially averaged climatology	0.005	(0.000–0.091)	0.002	(0.001–0.004)
	Temporally averaged climatology	0.005	(0.000–0.090)	0.000	(0.000–0.001)
	Full climatology	0.004	(0.000–0.080)	0.000	(0.000–0.001)
Band 4 (0.527)	No correction	0.054	(0.025–0.166)	0.007	(0.004–0.010)
	Pristine air	0.052	(0.024–0.164)	0.006	(0.002–0.009)
	Spatially averaged climatology	0.028	(0.001–0.139)	0.018	(0.015–0.022)
	Temporally averaged climatology	0.010	(0.000–0.117)	0.001	(0.000–0.004)
	Full climatology	0.008	(0.000–0.099)	0.001	(0.000–0.003)
Band 5 (0.372)	No correction	0.028	(0.018–0.061)	0.008	(0.007–0.009)
	Pristine air	0.019	(0.009–0.052)	0.002	(0.001–0.003)
	Spatially averaged climatology	0.012	(0.002–0.044)	0.008	(0.007–0.009)
	Temporally averaged climatology	0.003	(0.000–0.034)	0.000	(0.000–0.001)
	Full climatology	0.002	(0.000–0.029)	0.000	(0.000–0.001)
Band 7 (0.211)	No correction	0.032	(0.023–0.038)	0.012	(0.011–0.013)
	Pristine air	0.015	(0.006–0.021)	0.001	(0.000–0.002)
	Spatially averaged climatology	0.012	(0.003–0.018)	0.009	(0.008–0.009)
	Temporally averaged climatology	0.001	(0.000–0.009)	0.000	(0.000–0.001)
	Full climatology	0.001	(0.000–0.009)	0.000	(0.000–0.001)
NDVI (0.62)	No correction	0.058	(0.027–0.379)	0.011	(0.008–0.014)
	Pristine air	0.043	(0.013–0.364)	0.005	(0.002–0.008)
	Spatially averaged climatology	0.031	(0.001–0.347)	0.016	(0.011–0.023)
	Temporally averaged climatology	0.020	(0.000–0.329)	0.001	(0.000–0.004)
	Full climatology	0.015	(0.000–0.290)	0.001	(0.000–0.002)

[a]The presented four correction strategies are applicable to imagery for which the state of atmosphere at the time of acquisition is unknown. This table summarizes data presented in Figures 6–8.

[39] The reported discrepancies in AOD climatologies derived from two distinct data sets (both evaluated as generally adequate) illustrate the problem that the reflectance measurements do not provide enough information to unambiguously retrieve all the relevant parameters of aerosol, as this constituent exhibits great variability of physical properties, whereas the properties of gaseous atmosphere are well defined. Various simplifying assumptions have to be made in the retrieval process, which can lead to errors in the resulting products [e.g., *Kokhanovsky et al.*, 2007;

Table 3. Mean and Standard Deviation (SD) of Reflectance and NDVI of Pixels Common to 10 Landsat 7 Scenes (After Exclusion of Data Gaps and Clouds) at Low (500 ± 250 m) and High (4000 ± 250 m) Ground Elevation, Before and After Atmospheric Correction[a]

	Elevation 500 m		Elevation 4000 m	
Bands	TOA (mean ± SD)	Correction (mean ± SD)	TOA (mean ± SD)	Correction (mean ± SD)
Band 1	0.097 ± 0.026	0.018 ± 0.006	0.082 ± 0.008	0.038 ± 0.008
Band 2	0.074 ± 0.021	0.035 ± 0.004	0.080 ± 0.008	0.061 ± 0.008
Band 3	0.049 ± 0.019	0.024 ± 0.003	0.084 ± 0.013	0.077 ± 0.013
Band 4	0.248 ± 0.018	0.269 ± 0.019	0.175 ± 0.012	0.173 ± 0.012
Band 5	0.105 ± 0.010	0.112 ± 0.010	0.188 ± 0.020	0.191 ± 0.020
Band 7	0.037 ± 0.005	0.043 ± 0.004	0.116 ± 0.018	0.123 ± 0.019
NDVI	0.677 ± 0.096	0.834 ± 0.020	0.349 ± 0.090	0.388 ± 0.097

[a]This table summarizes data presented in Figure 9.

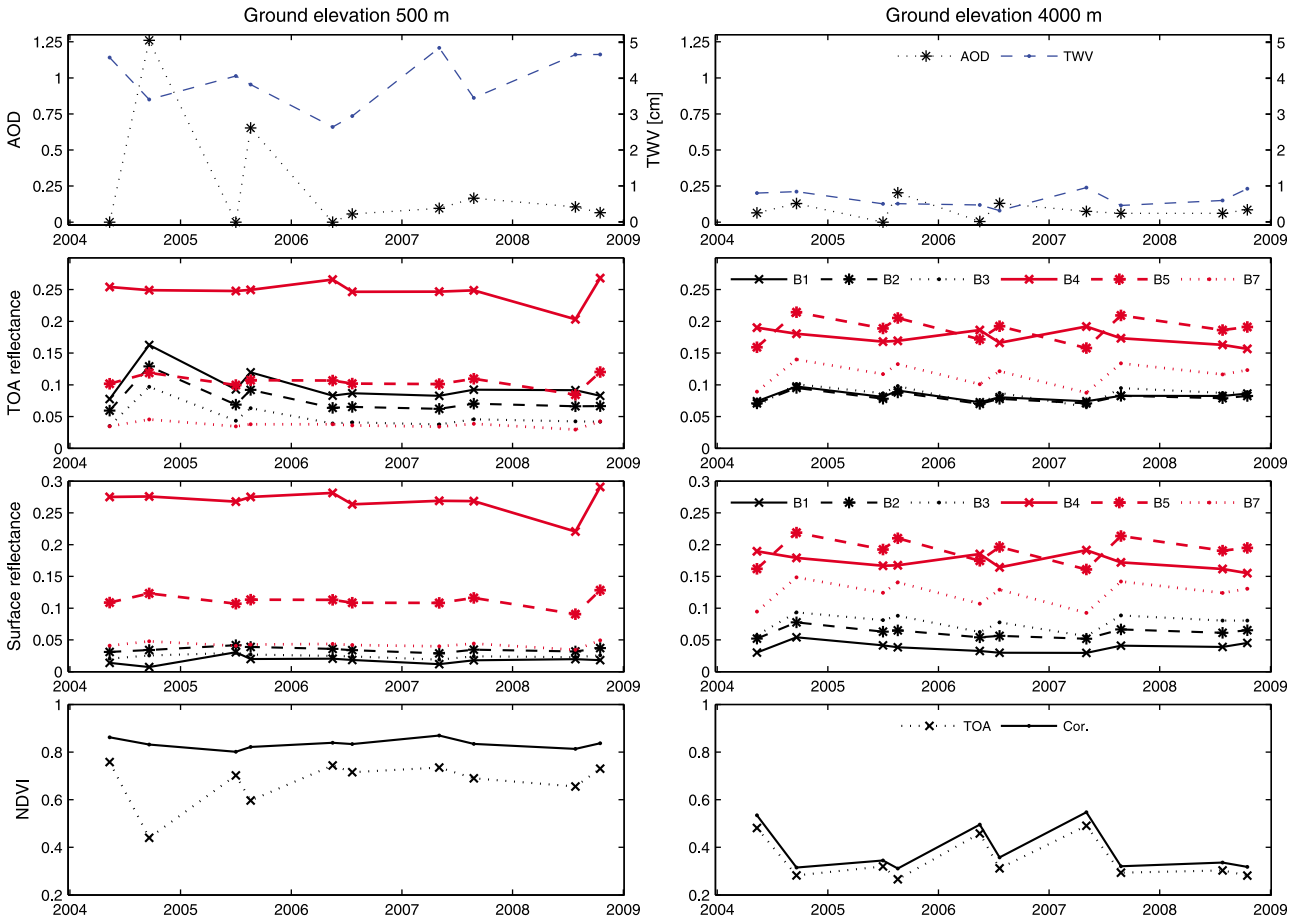

Figure 9. Key atmospheric properties (TWV, AOD), top-of-atmosphere reflectance, surface reflectance, and NDVI in time series comprising 10 Landsat 7 scenes. Plotted values represent mean values of pixels common to all scenes (after exclusion of data gaps and clouds), situated at low (500 ± 250 m, mainly forest) and high (4000 ± 250 m, mainly grassland) ground elevation.

Kokhanovsky et al., 2010b]. Moreover, subpixel cloud contamination is well known to lead to elevated AOD estimates and is likely to be more of a problem for AATSR than MODIS because of the coarser native spatial resolution [*Koren et al.*, 2008; *Wen et al.*, 2007]. This can be seen as a warning about the quality of AOD retrievals from fine-resolution Landsat-type data, which, in general, has significantly smaller radiometric accuracy than MODIS, or ATTSR. Fortunately, the methodologies to characterize atmospheric aerosol are continuously improving; for example, the MODIS collection 051 Deep Blue algorithm [*Hsu et al.*, 2004] significantly reduces the amount of gaps as it can be applied to bright reflecting surfaces. Nevertheless, the resulting data sets are likely to always be of lower spatial resolution than in the case of land surface imagery, and to contain more gaps.

[40] The proposed background + anomalies approach to map constituent distribution, which can be used to downscale and gap fill satellite atmospheric data, appeared as generally robust. Its most critical element is the constituent concentration at low elevations, which tends to be relatively high and more uncertain. This concentration determines the lapse rate across the elevation gradient because the upper elevational limit (near-zero concentration) is relatively stable. In this context, the frequent gaps in the elevational mid-domain (due to complex topography, frequent clouds, and their shadows) could be mitigated with the proposed approach. The usefulness of the background + anomalies approach is particularly clear in the case of TWV data, which are characterized by strong elevational gradients across the entire year. In the case of AOD, the application of the approach is more challenging due to the quality of AOD data, the relatively low mean coefficient of determination between AOD and ground elevation, and greater role of local anomalies. Nevertheless, in all cases, when elevation can explain some of the AOD spatial variability, the proposed approach is bound to yield more probable values than simple spatial interpolation. Moreover, the coincidence of low coefficient of determination with small contrast between low and high elevations speaks for the validity of the proposed approach because in such circumstances, the background concentration becomes a simple mean of similar and predominantly low measurements. In other words, the situation where the estimate of background concentration is negatively affected by many highly variable measurements is uncommon in the analyzed data set. Furthermore, certain factors of a technical nature can be expected to make the elevational gradient of AOD more elusive. For example, the precise mean elevation of relatively large grid boxes cannot

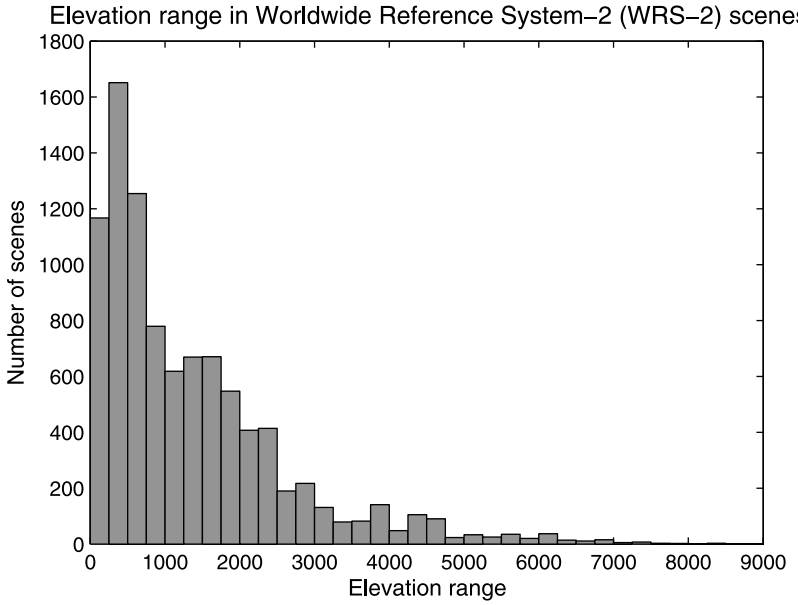

Figure 10. Elevation ranges in Landsat scenes across the Earth's land surface (Worldwide Reference System-2). Scenes that overlap with water by more than 95% were excluded.

be established, because only some of the underlying land area was used in the retrieval. In addition, the presented MODIS data suffer from region-specific positive bias of AOD over highly elevated land. On the other hand, the AOD gradients across elevation can be expected to be less pronounced than in the case of TWV because aerosols have poorer dispersal potential than gases and can have very localized sources. Moreover, a more efficient air mixing below the atmospheric boundary layer may weaken AOD elevational gradients near land surface. This phenomenon could be accounted for with a more complex model of AOD distribution [e.g., *He et al.*, 2008]; however, it would be difficult to validate such a model with the presented data, given its quality.

[41] The presented approach to atmospheric correction with atmosphere parameterization based on satellite data can be seen as an alternative to methods using image-based inference of atmospheric bias. However, these two approaches could as well complement each other. For example, the fine-resolution image-based estimates of AOD, which are more uncertain, could be calibrated using AOD coverages generated in the way proposed here. Moreover, image-based inference of AOD can be used to flag the presence of small-scale smoke plumes and similar phenomena.

[42] Despite some uncertainty in parameterization of the atmosphere, this study clearly shows that cyclic changes in atmospheric composition can cause apparent seasonality of vegetation indices. Such spurious effects could be confused with changes in the state of vegetation. Since the Landsat scene analyzed here overlaps with the Amazon basin, the presented findings contribute to the debate about drivers of the "Amazon green-up" [*Saleska et al.*, 2007] at times of low water availability. The causes of this phenomenon are likely to be complex, including changes in canopies [*Anderson et al.*, 2010], cloudiness [*Asner and Alencar*, 2010], but also image correction method [*Samanta et al.*, 2010].

[43] Although this study was based on a relatively small area (~200 × 200 km), its conclusions are likely to apply to other regions of Earth. Atmosphere parameterization based on satellite data could be useful over all land, whereas the proposed background + anomalies approach is mainly useful over rugged terrain. The analysis of elevational ranges in Landsat scenes across all land (Figure 10) showed that as much as half of the scenes cover elevational range of at least 1 km, which suggests relatively high demand for data gap filling and downscaling, and for taking account of atmospheric variability linked to altitude. Last, the negative effect of atmospheric bias can be expected to be more pronounced over areas situated further away from the equator, due to greater seasonal changes in illumination and generally higher solar zenith angles (although the amounts of water vapor are generally lower). This suggests that outside the tropics, atmospheric correction may yield greater benefits than those presented here.

[44] Overall, the presented evidence leads to the conclusion that the satellite-based atmospheric data available to date are likely to allow for an improvement in all fine-resolution imageries of land surface, regardless of acquisition date and place. Locally, the validity of this conclusion depends on the quality of satellite retrievals of relevant atmospheric constituents and the degree to which they have a regionally stable pattern of mean state and variability. Although these issues certainly require further investigation, the presented study can be seen as a case for routine atmospheric correction of land surface imagery (e.g., from Landsat satellites) performed by the data provider, rather than the end user, which would substantially improve the quality of commonly used data sets.

[45] **Acknowledgments.** We are very grateful to Giles Foody, Yadvinder Malhi, Soo Chin Liew, and two anonymous reviewers for useful suggestions on the manuscript. The research was supported financially by the Blue Moon Foundation.

References

Anderson, L. O., Y. Malhi, L. E. O. C. Aragão, R. Ladle, E. Arai, N. Barbier, and O. Phillips (2010), Remote sensing detection of droughts in Amazonian forest canopies, *New Phytol.*, *187*(3), 733–750.

Asner, G. P., and A. Alencar (2010), Drought impacts on the Amazon forest: The remote sensing perspective, *New Phytol.*, *187*(3), 569–578.

Bowman, K. P., and A. J. Krueger (1985), A global climatology of total ozone from the Nimbus 7 total ozone mapping spectrometer, *J. Geophys. Res.*, *90*(D5), 7967–7976, doi:10.1029/JD090iD05p07967.

Bush, M. B., M. R. Silman, C. McMichael, and S. Saatchi (2008), Fire, climate change and biodiversity in Amazonia: A Late-Holocene perspective, *Philos. Trans. R. Soc. B*, *363*(1498), 1795–1802, doi:10.1098/rstb.2007.0014.

Chander, G., B. L. Markham, and D. L. Helder (2009), Summary of current radiometric calibration coefficients for Landsat MSS, TM, ETM+, and EO-1 ALI sensors, *Remote Sens. Environ.*, *113*(5), 893–903, doi:10.1016/j.rse.2009.01.007.

Coppin, P., I. Jonckheere, K. Nackaerts, B. Muys, and E. Lambin (2004), Digital change detection methods in ecosystem monitoring: A review, *Int. J. Remote Sens.*, *25*(9), 1565–1596, doi:10.1080/0143116031000101675.

Forster, P., et al. (2007), Changes in atmospheric constituents and in radiative forcing, in *Climate Change 2007: The Physical Science Basis. Contribution of Working Group I to the Fourth Assessment Report of the Intergovernmental Panel on Climate Change*, edited by S. Solomon et al., pp. 129–234, Cambridge Univ. Press, Cambridge, U. K.

Gao, B. C., and Y. J. Kaufman (2003), Water vapor retrievals using moderate resolution Imaging spectroradiometer (MODIS) near-infrared channels, *J. Geophys. Res.*, *108*(D13), 4389, doi:10.1029/2002JD003023.

He, Q., C. Li, J. Mao, A. K.-H. Lau, and D. A. Chu (2008), Analysis of aerosol vertical distribution and variability in Hong Kong, *J. Geophys. Res.*, *113*, D14211, doi:10.1029/2008JD009778.

Hsu, N. C., T. Si-Chee, M. D. King, and J. R. Herman (2004), Aerosol properties over bright-reflecting source regions, *IEEE Trans. Geosci. Remote Sens.*, *42*(3), 557–569.

Kaufman, Y. J. (1985), The atmospheric effect on the separability of field classes measured from satellites, *Remote Sens. Environ.*, *18*(1), 21–34, doi:10.1016/0034-4257(85)90035-5.

Kaufman, Y. J., and B. C. Gao (1992), Remote-sensing of water-vapor in the near Ir from EOS/MODIS, *IEEE Trans. Geosci. Remote Sens.*, *30*(5), 871–884, doi:10.1109/36.175321.

Kokhanovsky, A. A., et al. (2007), Aerosol remote sensing over land: A comparison of satellite retrievals using different algorithms and instruments, *Atmos. Res.*, *85*(3–4), 372–394, doi:10.1016/j.atmosres.2007.02.008.

Kokhanovsky, A. A., V. P. Budak, C. Cornet, M. Z. Duan, C. Emde, I. L. Katsev, D. A. Klyukov, S. V. Korkin, L. C-Labonnote, B. Mayer, et al. (2010a), Benchmark results in vector atmospheric radiative transfer, *J. Quant. Spectrosc. Radiat. Transfer*, *111*(12–13), 1931–1946, doi:10.1016/j.jqsrt.2010.03.005.

Kokhanovsky, A. A., et al. (2010b), The inter-comparison of major satellite aerosol retrieval algorithms using simulated intensity and polarization characteristics of reflected light, *Atmos. Meas. Tech.*, *3*(4), 909–932, doi:10.5194/amt-3-909-2010.

Koren, I., L. Oreopoulos, G. Feingold, L. A. Remer, and O. Altaratz (2008), How small is a small cloud?, *Atmos. Chem. Phys.*, *8*(14), 3855–3864, doi:10.5194/acp-8-3855-2008.

Körner, C. (2007), The use of "altitude" in ecological research, *Trends Ecol. Evol.*, *22*(11), 569–574, doi:10.1016/j.tree.2007.09.006.

Kotchenova, S. Y., and E. F. Vermote (2007), Validation of a vector version of the 6s radiative transfer code for atmospheric correction of satellite data. Part II. Homogeneous Lambertian and anisotropic surfaces, *Appl. Opt.*, *46*(20), 4455–4464, doi:10.1364/AO.46.004455.

Kotchenova, S. Y., E. F. Vermote, R. Levy, and A. Lyapustin (2008), Radiative transfer codes for atmospheric correction and aerosol retrieval: Intercomparison study, *Appl. Opt.*, *47*(13), 2215–2226, doi:10.1364/AO.47.002215.

Levelt, P. F., G. H. J. Van den Oord, M. R. Dobber, A. Malkki, H. Visser, J. de Vries, P. Stammes, J. O. V. Lundell, and H. Saari (2006), The Ozone Monitoring Instrument, *IEEE Trans. Geosci. Remote Sens.*, *44*(5), 1093–1101, doi:10.1109/TGRS.2006.872333.

Levy, R. C., L. A. Remer, R. G. Kleidman, S. Mattoo, C. Ichoku, R. Kahn, and T. F. Eck (2010), Global evaluation of the Collection 5 MODIS dark-target aerosol products over land, *Atmos. Chem. Phys.*, *10*, 10,399–10,420, doi:10.5194/acp-10-10399-2010.

Livingston, J. M., et al. (2003), Airborne Sun photometer measurements of aerosol optical depth and columnar water vapor during the Puerto Rico Dust Experiment and comparison with land, aircraft, and satellite measurements, *J. Geophys. Res.*, *108*(D19), 8588, doi:10.1029/2002JD002520.

Llewellyn-Jones, D., M. C. Edwards, C. T. Mutlow, A. R. Birks, I. J. Barton, and H. Tait (2001), AATSR: Global-change and surface-temperature measurements from Envisat, *ESA Bull.*, *105*, 11–21.

Lu, D., and Q. Weng (2007), A survey of image classification methods and techniques for improving classification performance, *Int. J. Remote Sens.*, *28*(5), 823–870, doi:10.1080/01431160600746456.

Lyapustin, A., D. L. Williams, B. Markham, J. Irons, B. Holben, and Y. Wang (2004), A method for unbiased high-resolution aerosol retrieval from Landsat, *J. Atmos. Sci.*, *61*(11), 1233–1244, doi:10.1175/1520-0469(2004)061<1233:AMFUHA>2.0.CO;2.

Martonchik, J. V., D. J. Diner, K. A. Crean, and M. A. Bull (2002), Regional aerosol retrieval results from MISR, *IEEE Trans. Geosci. Remote Sens.*, *40*(7), 1520–1531, doi:10.1109/TGRS.2002.801142.

Myneni, R. B., and G. Asrar (1994), Atmospheric effects and spectral vegetation indexes, *Remote Sens. Environ.*, *47*(3), 390–402, doi:10.1016/0034-4257(94)90106-6.

Pettorelli, N., J. O. Vik, A. Mysterud, J. M. Gaillard, C. J. Tucker, and N. C. Stenseth (2005), Using the satellite-derived NDVI to assess ecological responses to environmental change, *Trends Ecol. Evol.*, *20*(9), 503–510, doi:10.1016/j.tree.2005.05.011.

Randel, W. J., R. S. Stolarski, D. M. Cunnold, J. A. Logan, M. J. Newchurch, and J. M. Zawodny (1999), Trends in the vertical distribution of ozone, *Science*, *285*(5434), 1689–1692, doi:10.1126/science.285.5434.1689.

Richter, R., D. Schlapfer, and A. Muller (2006), An automatic atmospheric correction algorithm for visible/NIR imagery, *Int. J. Remote Sens.*, *27*(10), 2077–2085, doi:10.1080/01431160500486690.

Saleska, S. R., K. Didan, A. R. Huete, and H. R. da Rocha (2007), Amazon forests green-up during 2005 drought, *Science*, *318*, 612–612.

Samanta, A., S. Ganguly, H. Hashimoto, S. Devadiga, E. Vermote, Y. Knyazikhin, R. R. Nemani, and R. B. Myneni (2010), Amazon forests did not green-up during the 2005 drought, *Geophys. Res. Lett.*, *37*, L05401, doi:10.1029/2009GL042154.

Sayer, A. M., G. E. Thomas, R. G. Grainger, E. Carboni, C. Poulsen, and R. Siddans (2011), Use of MODIS-derived surface reflectance data in the ORAC-AATSR aerosol retrieval algorithm: Impact of differences between sensor spectral response functions, *Remote Sens. Environ.*, in press.

Schmid, B., et al. (2009), Validation of aerosol extinction and water vapor profiles from routine Atmospheric Radiation Measurement Program Climate Research Facility measurements, *J. Geophys. Res.*, *114*, D22207, doi:10.1029/2009JD012682.

Thomas, G. E., C. A. Poulsen, A. M. Sayer, S. H. Marsh, S. M. Dean, E. Carboni, R. Siddans, and R. G. Grainger (2009), Oxford-RAL Aerosol and Cloud (ORAC): Aerosol retrievals from satellite radiometers, in *Aerosol Remote Sensing Over Land*, edited by A. A. Kokhanvosky and G. de Leeuw, pp. 193–226, Springer, Berlin, doi:10.1007/978-3-540-69397-0_7.

Turner, D. D., R. A. Ferrare, and L. A. Brasseur (2001), Average aerosol extinction and water vapor profiles over the Southern Great Plains, *Geophys. Res. Lett.*, *28*(23), 4441–4444, doi:10.1029/2001GL013691.

Vermote, E. F., N. El Saleous, C. O. Justice, Y. J. Kaufman, J. L. Privette, L. Remer, J. C. Roger, and D. Tanre (1997a), Atmospheric correction of visible to middle-infrared EOS-MODIS data over land surfaces: Background, operational algorithm and validation, *J. Geophys. Res.*, *102*(D14), 17,131–17,141, doi:10.1029/97JD00201.

Vermote, E. F., D. Tanre, J. L. Deuze, M. Herman, and J. J. Morcette (1997b), Second simulation of the satellite signal in the solar spectrum, 6s: An overview, *IEEE Trans. Geosci. Remote Sens.*, *35*(3), 675–686.

von Hoyningen-Huene, W., M. Freitag, and J. B. Burrows (2003), Retrieval of aerosol optical thickness over land surfaces from top-of-atmosphere radiance, *J. Geophys. Res.*, *108*(D9), 4260, doi:10.1029/2001JD002018.

Wen, G. Y., A. Marshak, R. F. Cahalan, L. A. Remer, and R. G. Kleidman (2007), 3-D aerosol-cloud radiative interaction observed in collocated MODIS and ASTER images of cumulus cloud fields, *J. Geophys. Res.*, *112*, D13204, doi:10.1029/2006JD008267.

Zelazowski, P. (2011). Contemporary and future extent of evergreen tropical forests: Insights from remote sensing and climate change simulations, Ph.D. thesis, Environmental Change Institute, Univ. of Oxford, Oxford, U. K.

R. G. Grainger and G. E. Thomas, Atmospheric, Oceanic, and Planetary Physics, Department of Physics, University of Oxford, Oxford, UK.

A. M. Sayer, Climate and Radiation Branch, Laboratory for Atmospheres, NASA Goddard Space Flight Center, Greenbelt, MD, USA.

P. Zelazowski, Environmental Change Institute, School of Geography and the Environment, University of Oxford, Oxford, UK. (p.zelazowski@gmail.com)